Intrinsic small polarons in rutile TiO_2

Shan Yang (杨山),[1,*] A. T. Brant,[2] N. C. Giles,[2] and L. E. Halliburton[1,†]
[1]*Department of Physics, West Virginia University, Morgantown, West Virginia 26505, USA*
[2]*Department of Engineering Physics, Air Force Institute of Technology, Wright-Patterson Air Force Base, Ohio 45433, USA*
(Received 6 February 2013; revised manuscript received 25 February 2013; published 7 March 2013)

Electron paramagnetic resonance (EPR) is used to identify the intrinsic electron small polaron in TiO_2 crystals having the rutile structure. These self-trapped electrons are produced at very low temperature with 442 nm laser light. The defects form when a Ti^{4+} ion at a regular lattice site traps an electron and converts to a Ti^{3+} ($3d^1$) ion. They become thermally unstable above ~15 K. An activation energy of 24 meV describes this "release" of the electrons (either by a hopping motion or directly to the conduction band). The g matrix is obtained from the angular dependence of the EPR spectrum. Principal values are 1.9807, 1.9786, and 1.9563 and principal axes are along high-symmetry directions in the crystal. The unpaired electron occupies an $|x^2 - y^2\rangle$ orbital where x and y are in the equatorial plane of the TiO_6 unit and y is the [001] direction. These intrinsic small polarons serve as a prototype for many of the defect-associated Ti^{3+} ions often observed in this material. They also can be used as a computational test case to evaluate the validity of different approximations presently being employed in density-functional-theory modeling of point defects in TiO_2 and other transition-metal oxides.

DOI: 10.1103/PhysRevB.87.125201 PACS number(s): 71.38.Ht, 76.30.Fc, 61.72.jn

I. INTRODUCTION

The self-trapped electron is an important and fundamental point defect in TiO_2 crystals. Computational studies predict the existence of this defect,[1–11] but there have been no definitive experimental verifications of its existence in rutile crystals until now. The focus of the present paper is the experimental observation and characterization of the intrinsic small polaron, i.e., a self-trapped electron, in TiO_2 (rutile) crystals. We produce this defect in the otherwise perfect TiO_2 lattice during excitation at low temperature with laser light. Below ~15 K, the electron is self-trapped at a Ti^{4+} ion and forms a stable Ti^{3+} ion (with a $3d^1$ configuration). After removing the laser light, the trapped electron is thermally released as the temperature is increased from 15 to 20 K. The thermal activation energy associated with this electron release is ~24 meV. These electrons then "move" through the crystal and recombine with the charge-compensating hole centers that are also formed during the initial illumination.

Electron paramagnetic resonance (EPR) has been widely used to investigate trapped electrons in nanoparticles and films of TiO_2 (both the rutile and anatase phases) and in rutile-structured bulk single crystals of TiO_2. This experimental technique offers high resolution and is able to detect small concentrations of paramagnetic defects.[12] The TiO_2 lattice is well-known for its ability to "trap" electrons as Ti^{3+} ions and thus form a large family of similar, yet slightly different, Ti^{3+}-related centers.[13–19] Many of the EPR studies in TiO_2 have focused on Ti^{3+} ions associated with oxygen vacancies, Ti^{3+} ions at interstitial sites, and Ti^{3+} ions at or very near the surface. In recent studies,[20–22] EPR has been combined with electron-nuclear double resonance (ENDOR) to identify a series of donor-bound small polarons in rutile-structured TiO_2 crystals. These neutral donors consist of Ti^{3+} ions at regular lattice sites with an adjacent F (on an oxygen site), H (in the form of an OH^- molecular ion), or Li (at an interstitial site).

In the present paper, EPR is used to identify and characterize the intrinsic self-trapped electron in commercial bulk TiO_2 (rutile) crystals. Illumination at 15 K or below with 442 nm laser light produces an EPR spectrum that has the same symmetry as a regular unperturbed Ti^{4+} site in the lattice. Its shallow nature, as indicated by the lack of thermal stability, and the absence of a symmetry-lowering nearby perturbation allow us to assign this spectrum to a Ti^{3+} ion (i.e., a self-trapped electron) in an otherwise perfect region of the crystal. This defect is appropriately referred to as an intrinsic small polaron.[23] Principal values and principal-axis directions of the g matrix are obtained from a complete set of angular dependence data. The EPR signal can be observed at temperatures as high as 20 K during illumination, but at this temperature it quickly decays when the laser light is removed. A series of isothermal decay curves taken in the 17–20 K temperature range are combined with a general-order-kinetics analysis to determine the activation energy that describes this release of electrons from the Ti^{3+} ions. After an illumination at 15 K, photoinduced holes that charge compensate the self-trapped electrons are located at M^{4+} transition-metal ions substituting for Ti^{4+} ions (where M is either Fe or Cr).[24–26] Optically excited electrons move from the deep singly ionized M^{3+} acceptors (that are introduced during growth) to the conduction band and leave behind trapped holes in the form of M^{4+} ions.

II. EXPERIMENT

The TiO_2 (rutile) crystals used in the present investigation were commercially grown at CrysTec (Berlin, Germany) by the Verneuil method. These tetragonal crystals belong to space group $P4_2/mnm$ (or equivalently, D_{4h}^{14}) and their lattice constants[27,28] are $a = 4.5937$ Å, $c = 2.9587$ Å, and $u = 0.30478$. As shown in Fig. 1, these crystals consist of slightly distorted TiO_6 octahedra. The octahedra are all equivalent, but they are alternately elongated in [110] and [$\bar{1}$10] directions (these two distinct TiO_6 units are related by 90° rotations about

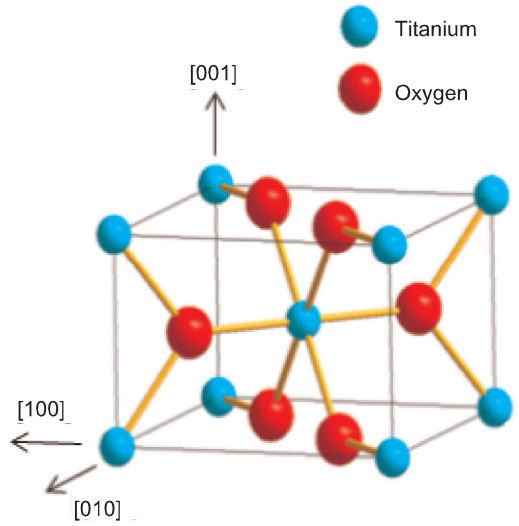

FIG. 1. (Color online) A schematic representation of the TiO_2 (rutile) lattice. One of the two equivalent, slightly distorted TiO_6 octahedra is shown.

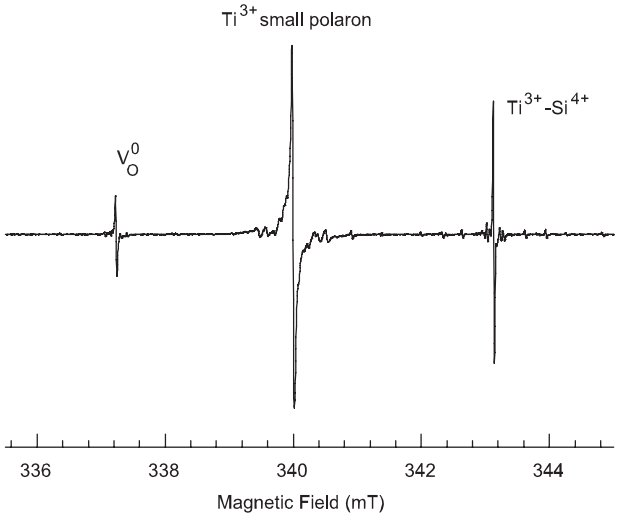

FIG. 2. Photoinduced EPR spectrum from a TiO_2 (rutile) crystal. These data were taken at 15 K during exposure to 442 nm laser light. The magnetic field was along the [001] direction and the microwave frequency was 9.309 GHz. The three signals, from low to high field, are from the neutral oxygen vacancy (V_O^0), the Ti^{3+} self-trapped electron, and the Ti^{3+}-Si^{4+} center.

the [001] direction). Because of these two different orientations of the TiO_6 octahedra, Ti^{3+} ions occupy two magnetically distinguishable, yet crystallographically equivalent sites in this lattice. In the present paper, EPR spectra from Ti^{3+} ions clearly show well-resolved splittings in their angular dependence that are attributable to these two sites. Local symmetry at a titanium ion site is orthorhombic. The six oxygen ions within an octahedron divide into two groups: two apical oxygen ions and four equatorial oxygen ions. At room temperature, the apical oxygen ions are 1.9800 Å from the central Ti^{4+} ion and the four equatorial oxygen ions are 1.9485 Å from the Ti^{4+} ion.[27] As is usually the case for commercially available rutile material, Fe^{3+} and Cr^{3+} ions are present in our as-received crystals with a combined concentration estimated to be a few parts per million.

A Bruker EMX spectrometer operating near 9.31 GHz was used to take the EPR data, while a helium-gas-flow system from Oxford Instruments maintained the sample temperature in the 4–30 K range. The samples used in these experiments had dimensions of $4 \times 2 \times 1.5$ mm^3. Precise values of the static magnetic field were obtained using a Bruker proton NMR gaussmeter. A small MgO crystal doped with Cr^{3+} ions was used to correct for the difference in magnetic field between the sample and the probe tip of the gaussmeter (the isotropic g value for Cr^{3+} in MgO is 1.9800). Narrow slots in the end of the Bruker TE_{102} rectangular microwave cavity allowed optical access to the sample. Approximately 15 mW of 442 nm light from a cw He-Cd laser was incident on the sample ($\sim 6 \times 10^{17}$ photons cm^{-2} s^{-1}) during the low-temperature excitations. An equilibrium concentration of photoinduced defects was reached in less than 2 min.

III. EPR RESULTS

Figure 2 shows the photoinduced EPR spectrum obtained from a nominally undoped TiO_2 (rutile) crystal. These data were taken at 15 K during illumination with 442 nm laser light. The magnetic field was along the [001] direction and the microwave power was low (1.5 μW) to avoid saturating the EPR signals. Three EPR signals are present, all related to Ti^{3+} ions. There were no EPR signals in this magnetic field region before the illumination. The line at 337.2 mT is the low-field component of the doublet assigned to the $S = 1$ neutral charge state of the oxygen vacancy and the line at 343.1 mT has been tentatively assigned to the Ti^{3+}-Si^{4+} center.[16] The line at 340.0 mT near the middle of Fig. 2 represents the intrinsic Ti^{3+} small polaron (i.e., the self-trapped electron) and is the subject of the present paper. The concentration of self-trapped electrons contributing to the EPR signal in Fig. 2 is estimated to be $\sim 2.0 \times 10^{16}$ cm^{-3}. In an earlier paper, Yang *et al.*[16] reported this EPR signal from the self-trapped electrons, but did not provide a detailed characterization of the defect.

All three of the electronlike signals in Fig. 2 have long spin-lattice relaxation times at low temperature. The oxygen vacancy and silicon-related centers are thermally more stable than the self-trapped electron and can be easily monitored at higher temperatures between 25 and 30 K where the microwave saturation effects are not as important. In contrast, the self-trapped electron with its lower thermal stability is only observed with low microwave power at temperatures near and below 20 K.

The self-trapped electrons can be produced at 15 K in our fully oxidized TiO_2 crystals by illuminating with below-band-gap light. Since the crystal as a whole must remain neutral, an equal number of trapped-hole centers must also be produced during the illumination. The self-trapped holes reported earlier by Yang *et al.*[29] are only stable below 10 K and thus are not candidates for these charge compensators. Instead, singly ionized deep acceptor impurity ions serve as the compensators. EPR signals observed near 82.0 and 133.5 mT (for a microwave frequency of 9.312 GHz) verify that isolated Fe^{3+} and Cr^{3+} ions, respectively, are present in our as-grown crystals.[24–26]

When a crystal is exposed to 442 nm light at 15 K, these impurity EPR signals decrease in intensity and the EPR signal from the self-trapped electrons appears (along with the EPR spectra of other trapped-electron centers). This suggests that a portion of these deep acceptors are being converted to Fe^{4+} and Cr^{4+} ions. The below-band-gap photons excite electrons from the Fe^{3+} and Cr^{3+} ions to the conduction band (by way of broad, but weak, absorption bands present below the TiO_2 band edge) and leave behind holes in the form of Fe^{4+} and Cr^{4+} ions. Some of the electrons entering the conduction band are then self-trapped at regular unperturbed titanium sites. Above-band-gap light (325 nm from the He-Cd laser) also produces the self-trapped electron EPR spectrum, but with a tenfold reduction in equilibrium concentration (compared to the 442 nm light) because of the smaller depth of penetration of the light. By using below-band-gap light, a uniform distribution of self-trapped electrons is achieved in the crystal. It is important to emphasize that the Fe^{3+} and Cr^{3+} ions, unintentionally present in as-grown crystals, play a critical role when laser light is used to produce the self-trapped electrons between 15 and 20 K in completely oxidized TiO_2 crystals.

A. *g* matrix

The *g* matrix of the self-trapped electron is determined from the angular dependence of its EPR spectrum. As shown in Fig. 3, line positions were measured as the magnetic field was rotated in the three high-symmetry planes of the crystal. The splitting into two branches in two of these three planes demonstrates that there are two magnetically inequivalent, but crystallographically equivalent, sites for the Ti^{3+} ions. The principal values of the *g* matrix are the same for the two Ti^{3+} ion sites, but the principal-axis coordinate systems have different orientations at the two sites (i.e., the two Ti^{3+} ions

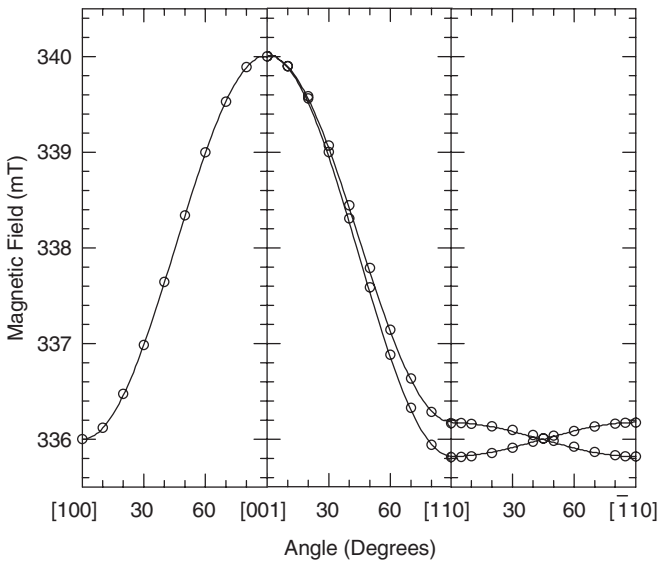

FIG. 3. Angular dependence of the EPR spectrum assigned to the self-trapped electron in a TiO_2 (rutile) crystal. Data were acquired in the three high-symmetry planes of the crystal. The discrete points are experimental results and the solid curves are computer generated using the *g*-matrix parameters in Table I.

are at the center of differently oriented TiO_6 octahedra in the lattice). Magnetic inequivalence of the Ti^{3+} ions occurs when the magnetic field makes different projections on these *g*-matrix principal-axis directions. For the $S = 1/2$ spectrum of the self-trapped electron, this magnetic inequivalence causes two lines to appear for some of the directions of magnetic field. As illustrated in Fig. 3, the two orientations of the self-trapped electron in TiO_2 are magnetically equivalent when the magnetic field is along the [100], [010], and [001] directions and also when the magnetic field is rotated from [001] toward either [100] or [010]. For all other directions of magnetic field, there are two lines in the spectrum due to the two magnetically inequivalent orientations of the Ti^{3+} ions.

The following spin Hamiltonian, containing only the electron Zeeman term, describes the angular dependence of the EPR spectrum:

$$\mathbf{H} = \beta \mathbf{S} \cdot \mathbf{g} \cdot \mathbf{B}. \tag{1}$$

Here, β is the Bohr magneton, **S** is the electron spin, and **B** is the magnetic field. A "turning point" occurs in Fig. 3 when the magnetic field is along the [001] direction. Thus, one of the principal axes of the *g* matrix must be along this direction. The other two principal axes must be in the basal plane. Turning points in this plane occur when the magnetic field is along the [110] and [$\bar{1}$10] directions (see the right panel in Fig. 3), and these directions are the remaining two principal axes of the *g* matrix. Having principal axes along high-symmetry directions supports our assignment of the EPR spectrum to intrinsic self-trapped electrons. Impurities such as Na^+, K^+, and Ca^{2+} are present in trace amounts in TiO_2 crystals, but it is unlikely that one of them is adjacent to our unpaired spin. A neighboring alkali or alkaline-earth ion at an interstitial site would cause deviations in the principal-axis directions of the *g* matrix similar to those previously observed for small polarons associated with hydrogen and lithium in TiO_2.[21,22] An alkaline-earth impurity (e.g., a Ca^{2+} ion) could also substitute for a Ti^{4+} ion, but it would then serve as a trapping site for a hole on a neighboring oxygen ion instead of a trapping site for an electron.

Once the principal axes are identified, the principal values of the *g* matrix are then obtained by measuring three lines (the one line in the EPR spectrum taken with the field along the [001] direction and the two lines in the EPR spectrum taken with the field along the [110] direction). These three magnetic fields, and their corresponding microwave frequencies, give the three principal values listed in Table I. The solid curves in Fig. 3 were computer generated using Eq. (1) and the results in Table I.

TABLE I. The *g* matrix for the self-trapped electron in TiO_2 (rutile). Principal-axis directions refer to the TiO_6 octahedron illustrated in Fig. 1. From the angular dependence results, it is impossible to determine which principal value (1.9807 or 1.9786) has its principal axis along the [110] direction. The estimated error is ± 0.0001 for the principal values and $\pm 1^\circ$ for the directions of the principal axes.

	Principal value	Principal-axis direction
g_1	1.9807 (or 1.9786)	[110]
g_2	1.9786 (or 1.9807)	[$\bar{1}$10]
g_3	1.9563	[001]

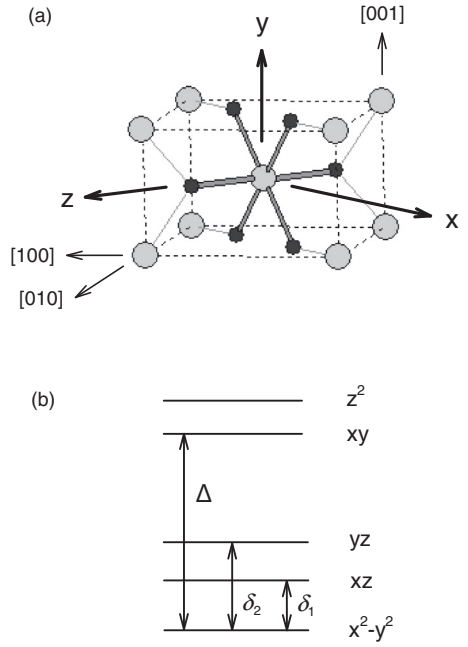

FIG. 4. (a) A distorted TiO_2 octahedron with the Ti^{3+} ion representing the self-trapped electron at the center. The labeled x,y,z coordinate system is used to describe the d orbitals. (b) Relative ordering in energy of the d orbitals on the Ti^{3+} ion.

The excellent agreement in Fig. 3 between experiment and calculation verifies that the correct set of g-matrix parameters have been determined.

The principal axes associated with the 1.9807 and 1.9786 principal values are in the basal plane, but we cannot experimentally determine which of these values has its associated principal axis pointing toward the apical oxygen neighbor in the TiO_6 octahedron and which lies between the two equatorial oxygen neighbors. This unresolved question (i.e., this choice) concerning the assignment of these two principal values to specific principal-axis directions is noted in Table I. Fortunately, the two principal values are similar in magnitude and the choice of directions has no significant effect on the model of the defect or on our interpretation of the g matrix. In the recent studies[20–22] of donor-bound small polarons in TiO_2 (i.e., the Ti^{3+} ions associated with F, H, or Li), similar questions about the matching of g-matrix principal values and principal-axis directions were resolved by finding agreement with the direction of the unique axis of the anisotropic (dipole-dipole) part of the donor hyperfine matrix.

The measured g matrix of the self-trapped electron (in Table I) provides information about the $3d$ orbitals associated with the Ti^{3+} ion. Figure 4(a) shows one of the two equivalent distorted TiO_6 octahedra with the Ti^{3+} ion at the center and the six nearest-neighbor oxygen ions. The x,y,z coordinate system in Fig. 4(a) has x along the $[\bar{1}10]$ direction, y along the [001] direction, and z along the [110] direction. The five atomic d orbitals can be written as

$$|xy\rangle = -\frac{i}{\sqrt{2}}(|2,2\rangle - |2,-2\rangle), \tag{2}$$

$$|xz\rangle = \frac{1}{\sqrt{2}}(|2,-1\rangle - |2,1\rangle), \tag{3}$$

$$|yz\rangle = \frac{i}{\sqrt{2}}(|2,-1\rangle + |2,1\rangle), \tag{4}$$

$$|x^2-y^2\rangle = \frac{1}{\sqrt{2}}(|2,2\rangle + |2,-2\rangle), \tag{5}$$

$$|z^2\rangle = |2,0\rangle. \tag{6}$$

The x and y axes in Fig. 4(a) do not point toward the nearest-neighbor oxygen ions. This choice of coordinate system, when coupled with the positions of the six nearest-neighbor negative oxygen ions and the ten next-nearest-neighbor positive titanium ions, gives rise to the relative ordering of energy levels shown in Fig. 4(b) for the five d orbitals. The $|x^2-y^2\rangle$ orbital is lowest in energy and the $|z^2\rangle$ orbital is highest in energy. The Ti^{3+} ion has six nearest-neighbor Ti^{4+} ions in the x-y plane in Fig. 4(a); four are shown and two are not shown. These latter two Ti^{4+} ions are along the [001] direction, directly above and below the Ti^{3+} ion. The relative positions of these six positive ions are the reason the $|x^2-y^2\rangle$ orbital is lowest in energy (i.e., the Ti^{4+} ions attract the negative charge located in the lobes of this d orbital).

The g matrix for an electron in an $|x^2-y^2\rangle$ orbital is given to first order by the following expressions.[30] We do not consider the small amount of mixing of the $|x^2-y^2\rangle$ and $|z^2\rangle$ orbitals that may occur in the orthorhombic crystal field of the rutile lattice.[31] (This mixing does not occur in cubic and tetragonal fields.)

$$g = g_e\hat{1} + 2\lambda\hat{\Lambda} \quad \text{where} \quad \Lambda_{ij} = -\sum_{n\neq G}\frac{\langle G|L_i|n\rangle\langle n|L_j|G\rangle}{E_n - E_G}. \tag{7}$$

The equation for Λ_{ij} involves matrix elements of the orbital momentum operators L_i ($i = x$, y, and z) between the ground state G, with energy E_G, and the four higher states n, with energies E_n. Principal values of the g matrix are obtained by evaluating these matrix elements.

$$g_x = g_e - \frac{2\lambda}{\delta_2}, \quad g_y = g_e - \frac{2\lambda}{\delta_1}, \quad g_z = g_e - \frac{8\lambda}{\Delta}. \tag{8}$$

The energy differences δ_1, δ_2, and Δ are illustrated in Fig. 4(b). In Eq. (8), $g_e = 2.0023$ and λ is the spin-orbit coupling constant ($+154$ cm^{-1} for a free Ti^{3+} ion). To account for covalency, an orbital reduction factor k is introduced that reduces the spin-orbit constant ($\lambda' = k\lambda$). We assign a value of 0.6 to k, which makes $\lambda' = 92.4$ cm^{-1}. In Eq. (8), we use $g_x = 1.9786$, $g_y = 1.9563$, and $g_z = 1.9807$ (from Table I) and replace λ with λ'. Solving for the separations in energy gives $\delta_1 = 4017$ cm^{-1}, $\delta_2 = 7797$ cm^{-1}, and $\Delta = 34\,222$ cm^{-1}. The other choice for g_x and g_z (interchanging 1.9786 and 1.9807) gives $\delta_2 = 8556$ cm^{-1} and $\Delta = 31\,190$ cm^{-1} and leaves δ_1 unchanged. For either choice, the values of δ_2 and Δ are similar and the ordering of the energy levels in Fig. 4(b) remains the same.

B. Thermal activation energy

After the laser light is removed, the EPR signal from the self-trapped electrons rapidly decreases in intensity if the temperature is between 15 and 20 K. Figure 5 shows four decay curves taken at specific temperatures in this range. These

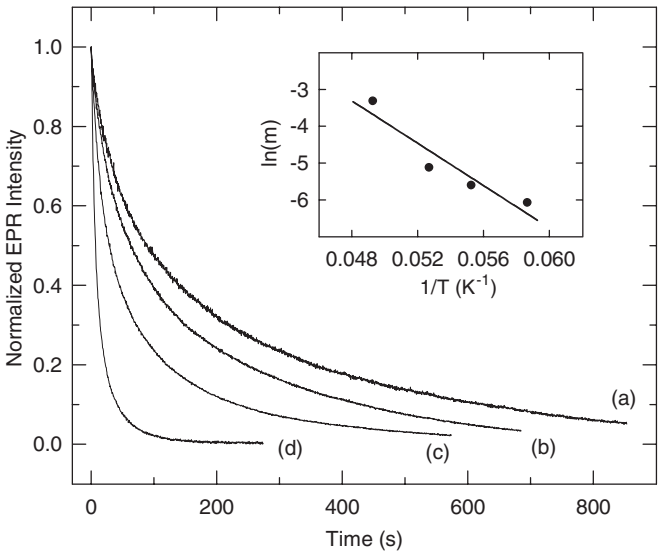

FIG. 5. Isothermal decays of the self-trapped-electron EPR signal. The magnetic field was held constant at the peak of the EPR signal and its decay was monitored as a function of time after removing the laser light. Temperatures for the individual decay curves were (a) 17.0, (b) 18.1, (c) 19.0, and (d) 20.3 K. The inset shows the plot of $\ln(m)$ versus $1/T$ used to obtain the activation energy E.

data were acquired by fixing the magnetic field at the peak of the EPR signal and then continually monitoring the intensity as a function of time after turning off the laser light. The temperature was kept constant (within ± 0.2 K) while taking a set of decay data. For each of the temperatures in Fig. 5, the laser was initially left on until an equilibrium concentration of self-trapped electrons was reached. The equilibrium concentrations were 2.0×10^{16} cm^{-3}, 1.8×10^{16} cm^{-3}, 1.2×10^{16} cm^{-3}, and 6.8×10^{15} cm^{-3} at 17.0, 18.1, 19.0, and 20.3 K, respectively. As expected, these equilibrium values decrease with increasing temperature. In general, the observed equilibrium concentrations of self-trapped electrons in our samples represent a balance between two primary competing mechanisms: (1) the production rate which depends on the intensity of the incident laser beam and (2) the decay rate which depends on temperature.

Single exponentials did not provide good fits to the decay curves in Fig. 5. Thus, a general-order kinetics model,[32–34] which takes into account the retrapping (and/or hopping) of the electrons, was used to analyze these data and extract an activation energy. The starting point in this analysis is the differential equation

$$\frac{dn}{dt} = -s' n^b \exp(-E/kT), \tag{9}$$

where n is the concentration of defects and b is a parameter which describes the order of the kinetics. Other parameters are the activation energy E, the temperature T, and a prefactor s' (note that s' does not have units of inverse seconds). The solution to Eq. (9) is

$$n(t) = n_0\left[1 + s' n_0^{b-1}(b-1)\exp(-E/kT)t\right]^{b-1}, \tag{10}$$

where n_0 is the initial concentration of self-trapped electrons (i.e., the concentration present at the time the laser light is removed). Equation (10) is then rewritten in the following form:

$$\left(\frac{n}{n_0}\right)^{1-b} = \left[1 + s' n_0^{b-1}(b-1)\exp(-E/kT)t\right]. \tag{11}$$

A plot of $(n/n_0)^{1-b}$ versus time was made for each set of decay data in Fig. 5. For each plot, the value of b was adjusted until a straight line emerged. As expected, these four values of b were similar and their average was $b = 1.38$ (with a variance of 0.0071). This value of b indicates a decay process between first and second order. Each of the four straight lines has a different slope. These slopes, according to Eq. (11), are

$$m = s' n_0^{b-1}(b-1)\exp(-E/kT). \tag{12}$$

Equation (12) is rewritten in the following form by taking the natural logarithm of each side:

$$\ln(m) = \ln\left[s' n_0^{b-1}(b-1)\right] - \frac{E}{kT}. \tag{13}$$

The final step is to make a plot of $\ln(m)$ versus $1/T$ (this plot contains four points, one for each decay curve, and is shown as an inset to Fig. 5). The slope of the best-fit straight line in the inset is $-E/k$. Using the decay data in Fig. 5 and following the procedure outlined above gives an activation energy of $E = 24 \pm 5$ meV. Our thermal decay results do not identify the primary physical mechanism by which the self-trapped electrons decay. An electron may hop from titanium to titanium until it reaches a trapped hole, or an electron may be thermally excited directly to the conduction band and then recombine with a trapped hole. It is possible that both of these processes have reasonable probabilities for occurrence in this 15–20 K temperature region.

IV. SUMMARY

The present investigation provides direct experimental evidence for the existence of self-trapped electrons in rutile crystals and thus supports the many recent density-functional-theory studies that have predicted the presence of these defects in TiO_2. Illumination at 15 K with 442 nm laser light produces the intrinsic small polarons in the TiO_2 (rutile) crystals. The charge-compensating trapped-hole centers, produced at the same time, are substitutional Fe^{4+} and Cr^{4+} ions. The EPR spectrum of these Ti^{3+} ($3d^1$) ions exhibits the same symmetry as the lattice and an analysis of the g matrix verifies that the unpaired spin occupies an $|x^2 - y^2\rangle$ orbital. These self-trapped electrons become thermally unstable above 15 K and an activation energy of 24 meV describes their decay (by hopping or ionization). Even at room temperature, illumination with near-band-edge light will produce these intrinsic polarons, but they will be highly mobile and will rapidly recombine with photoinduced holes or migrate to more stable trapping sites.

ACKNOWLEDGMENT

One of the authors (A.T.B.) acknowledges the support of the National Research Council.

*Present address: Mechanical and Aerospace Engineering Department, Case Western Reserve University, Cleveland, OH.
†Corresponding author: Larry.Halliburton@mail.wvu.edu

[1]A. Janotti, C. Franchini, J. B. Varley, G. Kresse, and C. G. Van de Walle, Phys. Status Solidi RRL **7**, 199 (2013).
[2]P. Deák, B. Aradi, and T. Frauenheim, Phys. Rev. B **86**, 195206 (2012).
[3]H.-Y. Lee, S. J. Clark, and J. Robertson, Phys. Rev. B **86**, 075209 (2012).
[4]T. Yamamoto and T. Ohno, Phys. Chem. Chem. Phys. **14**, 589 (2012).
[5]C. Di Valentin and A. Selloni, J. Phys. Chem. Lett. **2**, 2223 (2011).
[6]J. Stausholm-Møller, H. H. Kristoffersen, B. Hinnemann, G. K. H. Madsen, and B. Hammer, J. Chem. Phys. **133**, 144708 (2010).
[7]B. J. Morgan and G. W. Watson, Phys. Rev. B **80**, 233102 (2009).
[8]C. Di Valentin, G. Pacchioni, and A. Selloni, J. Phys. Chem. C **113**, 20543 (2009).
[9]B. J. Morgan, D. O. Scanlon, and G. W. Watson, J. Mater. Chem. **19**, 5175 (2009).
[10]E. Finazzi, C. Di Valentin, G. Pacchioni, and A. Selloni, J. Chem. Phys. **129**, 154113 (2008).
[11]N. A. Deskins and M. Dupuis, Phys. Rev. B **75**, 195212 (2007).
[12]J.-M. Spaeth and H. Overhof, *Point Defects in Semiconductors and Insulators: Determination of Atomic and Electronic Structure from Paramagnetic Hyperfine Interactions*, Springer Series of Materials Science Vol. 51 (Springer-Verlag, Berlin, 2003).
[13]S. Livraghi, M. Chiesa, M. C. Paganini, and E. Giamello, J. Phys. Chem. C **115**, 25413 (2011).
[14]S. Livraghi, S. Maurelli, M. C. Paganini, M. Chiesa, and E. Giamello, Angew. Chem., Int. Ed. **50**, 8038 (2011).
[15]I. R. Macdonald, R. F. Howe, X. Zhang, and W. Zhou, J. Photochem. Photobiol., A **216**, 238 (2010).
[16]S. Yang, L. E. Halliburton, A. Manivannan, P. H. Bunton, D. B. Baker, M. Klemm, S. Horn, and A. Fujishima, Appl. Phys. Lett. **94**, 162114 (2009).
[17]F. D. Brandao, M. V. B. Pinheiro, G. M. Ribeiro, G. Medeiros-Ribeiro, and K. Krambrock, Phys. Rev. B **80**, 235204 (2009).
[18]A. M. Czoska, S. Livraghi, M. Chiesa, E. Giamello, S. Agnoli, G. Granozzi, E. Finazzi, C. Di Valentin, and G. Pacchioni, J. Phys. Chem. C **112**, 8951 (2008).
[19]M. Aono and R. R. Hasiguti, Phys. Rev. B **48**, 12406 (1993).
[20]S. Yang and L. E. Halliburton, Phys. Rev. B **81**, 035204 (2010).
[21]A. T. Brant, S. Yang, N. C. Giles, and L. E. Halliburton, J. Appl. Phys. **110**, 053714 (2011).
[22]A. T. Brant, N. C. Giles, and L. E. Halliburton, J. Appl. Phys. **113**, 053712 (2013).
[23]A. L. Shluger and A. M. Stoneham, J. Phys.: Condens. Matter **5**, 3049 (1993).
[24]H. J. Gerritsen, S. E. Harrison, H. R. Lewis, and J. P. Wittke, Phys. Rev. Lett. **2**, 153 (1959).
[25]D. L. Carter and A. Okaya, Phys. Rev. **118**, 1485 (1960).
[26]G. J. Lichtenberger and J. R. Addison, Phys. Rev. **184**, 381 (1969).
[27]S. C. Abrahams and J. L. Bernstein, J. Chem. Phys. **55**, 3206 (1971).
[28]C. J. Howard, T. M. Sabine, and F. Dickson, Acta Crystallogr. Sect. B **47**, 462 (1991).
[29]S. Yang, A. T. Brant, and L. E. Halliburton, Phys. Rev. B **82**, 035209 (2010).
[30]J. E. Wertz and J. R. Bolton, *Electron Spin Resonance: Elementary Theory and Practical Applications* (McGraw-Hill, New York, 1972), pp. 278–281.
[31]R. Gallay, J. J. van der Klink, and J. Moser, Phys. Rev. B **34**, 3060 (1986).
[32]S. W. S. McKeever, *Thermoluminescence of Solids* (Cambridge University Press, Cambridge, Great Britain, 1985), pp. 98–99.
[33]C. E. May and J. A. Partridge, J. Chem. Phys. **40**, 1401 (1964).
[34]J. S. Nagpal and S. P. Kathuria, Int. J. Appl. Radiat. Isot. **35**, 495 (1984).